Modal and transient dynamics of jet flows

Xavier Garnaud, Lutz Lesshafft, Peter Schmid, Patrick Huerre

Modal and transient dynamics of jet flows

X. Garnaud,[1, a)] L. Lesshafft,[1] P.J. Schmid,[1] and P. Huerre[1]
LadHyX, Ecole Polytechnique – CNRS, 91128 Palaiseau, France.

The linear stability dynamics of incompressible and compressible isothermal jets are investigated by means of their optimal initial perturbations and of their temporal eigenmodes. The transient growth analysis of optimal perturbations is robust and allows physical interpretation of the salient instability mechanisms. In contrast, the modal representation appears to be inadequate, as neither the computed eigenvalue spectrum nor the eigenmode shapes allow a characterization of the flow dynamics in these settings. More surprisingly, numerical issues also prevent the reconstruction of the dynamics from a basis of computed eigenmodes. An investigation of simple model problems reveals inherent problems of this modal approach in the context of a stable convection-dominated configuration. In particular, eigenmodes may exhibit an exponential growth in the streamwise direction even in regions where the flow is locally stable.

I. INTRODUCTION

Jets are known to sustain large-scale perturbation structures, both in the laminar and turbulent flow regime. These structures are commonly interpreted as wavepackets developing within a laminar steady base state, or a turbulent mean flow, due to inflectional instability mechanisms. The spatial shape of the wavepacket envelope then depends on the downstream development of the base or mean flow. In order to fully account for the effects of non-parallelism, the present study seeks to identify wavepacket structures in the form of temporal eigenmodes of the linearized equations of motion in a two-dimensional domain. Linear "global modes" of this kind have been investigated for a large variety of flow configurations in recent years; examples include vortex shedding in the cylinder wake[1] or in a three-dimensional jet in crossflow[2], and the flapping of a separated boundary layer[3]. Weakly nonlinear flow dynamics may in some cases be described by a combination of several dominant global modes[4,5]; furthermore, passive[6] as well as active[7] control strategies for the suppression of flow oscillations have been devised based on the knowledge of the global mode spectrum. However, Barbagallo *et al.*[8] showed that a model reduction based on eigenmodes successfully captures the unstable structures but fails to represent the stable dynamics.

All of the above examples represent oscillator-type flows, where intrinsic flow oscillations observed in the nonlinear regime are found to be linked to the presence of at least one unstable linear global mode. In open shear flows, global instability is typically associated with the presence of a locally absolutely unstable flow region[9], although feedback mechanisms may also be responsible for the flow destabilization. In contrast, amplifier-type flows are characterized by a stable global eigenspectrum. Consistent with the notion of local convective instability, non-normal interaction of stable global modes may give rise to transient perturbation growth[10], but ultimately all perturbations decay in time. Jets, unless sufficiently hot[11,12], are prominent examples of amplifier-type flows. Crow & Champagne[13] measured the flow response in low-Mach number turbulent jets as a function of the forcing frequency, and found maximum amplification to occur at a Strouhal number of 0.3. This approximate value for the *preferred mode* has been confirmed in numerous later studies to be remarkably universal over a large range of operating conditions, even in the supersonic regime[14]. Huerre & Monkewitz[9] hypothesized that the preferred mode was the manifestation of a "slightly damped oscillator" character of the flow, i.e. that the strong flow response may be interpreted as a resonance of the least stable global mode in the presence of external

[a)] Electronic mail: garnaud@ladhyx.polytechnique.fr

forcing. Such an eigenmode has been identified by Cooper & Crighton[15] by extending the dispersion relation of the local shear-layer mode into the complex X-plane. The authors report a Strouhal number based on the diameter of 0.44 for this mode, in agreement with experimental observations[16]. This analysis is based on the hypothesis of the contribution of one single local mode to the global response and of a slow streamwise development of the flow.

Motivated by these results, the first objective of the present study is to compute the global spectrum of subsonic jets. A laminar steady state as well as a turbulent mean flow are considered in the incompressible limit, and the turbulent mean flow is further investigated in the compressible setting at a Mach number of 0.75.

Stable global spectra have been successfully computed for supersonic jets by Nichols & Lele[17,18]. In weakly non-parallel laminar settings, these calculations required extremely large numerical domains, extending over up to 800 jet radii in the downstream direction, in order to capture the wavepacket maximum and reach convergence. In turbulent mean flows obtained from Reynolds averaged calculations, the dominant modes were sufficiently localized near the nozzle to be accurately resolved on much shorter domains. However, difficulties with the computation of stable global modes have been reported for a variety of flow configurations. Barkley *et al.*[19] obtained easily converged modes that are localized within the recirculation bubbles behind a backward-facing step, but no convergence was achieved for a family of stable modes exhibiting spatial growth far downstream of the step; these modes therefore were not further explored. Similar problems were encountered in planar wakes with surface tension[20,21]. In a flat plate boundary layer[22], all modes are stable and spatially growing. Convergence with respect to the domain length was achieved in this case through the use of carefully designed boundary conditions, based on the local dispersion relation. Amplitudes at the in- and outflow differed by two orders of magnitude. Much larger variations occurred in the analysis of a Batchelor vortex by Heaton *et al.*[23]; amplitude differences on the order of 10^6 were found to prevent convergence. The second and principal objective of the present paper is to expose the root cause for such computational problems of stable global modes, and to delineate circumstances under which convergence may be impossible to achieve.

It has been shown that individual eigenmodes may carry a limited physical meaning in the context of amplifier flows and that non-modal stability analyses are more suitable[24,25] to represent instability features in this case. An eigenmode representation of the dynamics can however be used to carry out these analyses, and previous studies have shown that this provides a robust means of analyzing non-normal effects[22,26] as well as of performing control[7] for weakly unstable flows. Optimal perturbations are therefore computed in order to characterize transient growth phenomena in jets. Results obtained using both an adjoint method[27] and a modal representation of the propagator[28] are discussed.

The significance and challenges of a modal representation of the dynamics for advection dominated flows is first investigated by means of model systems in § II. The flow configuration of a round jet with a solid nozzle is then presented in § III, together with the numerical procedure and the different base flows that are investigated. The results of optimal perturbation (§ IV) and eigenmode (§ V) computations are then presented. Although most of the discussion is established in the context of incompressible flows, compressibility effects are also mentioned. Conclusions are offered in § VII.

II. MODEL PROBLEMS: EIGENMODES OF ADVECTIVE SYSTEMS

Reddy & Trefethen[29] investigated the features of the spectrum and pseudo-spectrum of a 1D convection-diffusion problem with homogeneous Dirichlet conditions at the inflow and outflow, a well posed Sturm-Liouville type of problem. The eigenmodes exhibit an exponential spatial growth, and a boundary layer forms at the outflow. In contrast in the model under consideration in Cossu & Chomaz[30] eigenmodes have a Gaussian envelope. The two models presented below aim at reproducing some of the features of a flow where instability mechanisms act in an upstream region, creating structures that are convected

downstream by a neutrally stable flow. These models show features similar to the problem considered by Reddy & Trefethen and provide an understanding of the relationship between the decay rate of a mode, its spatial structure and local instability features.

A. Advection equation with upstream boundary forcing

The simplest possible model for the evolution of perturbations in an advection-dominated flow is given by a pure advection equation with one spatial direction x and a constant advection velocity $U_0 > 0$. The system is forced by an unsteady upstream boundary condition with its own dynamics,

$$\frac{\partial \psi}{\partial t}(x,t) + U_0 \frac{\partial \psi}{\partial x}(x,t) = 0 \qquad x > 0, \tag{1a}$$

$$\psi(0,t) = \psi_0(t), \tag{1b}$$

$$\dot{\psi}_0(t) = -a\psi_0(t) \qquad a \in \mathbb{C}. \tag{1c}$$

The dynamics of this system are imposed by the linear ordinary differential equation (1c). The system (1) only has one single mode of the form $\psi(x,t) = \widetilde{\psi}(x)\exp(-\mathrm{i}\omega t)$, with eigenvector $\widetilde{\psi}(x)$ and eigenvalue ω given by

$$\widetilde{\psi}(x) = \exp\left(\frac{a}{U_0}x\right), \qquad \omega = -\mathrm{i}a. \tag{2}$$

If the system is stable, $a_r \geq 0$ (subscripts $_r$ and $_i$ denote, respectively, the real and imaginary parts of complex scalars and vectors), the amplitude of the mode grows exponentially in x and diverges as $x \to \infty$. A lower advection velocity U_0 leads to stronger spatial growth of $\widetilde{\psi}(x)$.

It is quite clear from this simple example how a temporally decaying source of perturbations under pure advection gives rise to a spatially growing structure, since all perturbations generated at a later time must be exponentially smaller than those generated earlier. Furthermore, this model also serves to exemplify the occurrence of spurious numerical modes. If (1) is discretized using a first-order upwind scheme on a uniform mesh, the mode (2) is recovered independently of the size of the numerical domain, but a second eigenvalue is found as $-1/h$, where h is the grid spacing. The corresponding spatial structure is localized at the outflow discretization point. If a general non-uniform mesh with n points is used, then n distinct modes exist, localized anywhere on the grid. In this particular example, $n-1$ of them have no physical meaning because they do not correspond to modes of the continuous problem. In a more general case where no *a priori* knowledge about the modal structure is available, care must be taken with numerically computed modes. Although the discretization method is suitable for transient problems, it is possible that even the least stable modes computed numerically may have no physical meaning.

B. Unforced advection–diffusion–reaction equation

It may be argued that the above model is indeed too simple for a comparison with jet dynamics, since information can only propagate downstream. This property, however, is not the cause for the exponential spatial growth. A similar reasoning can be applied to the linear advection–diffusion–reaction equation (also referred to as linear Ginzburg–Landau equation) , given as

$$\frac{\partial \psi}{\partial t} + U_0 \frac{\partial \psi}{\partial x} = -a(x)\psi + \frac{\partial^2 \psi}{\partial x^2} \qquad x > 0, \tag{3a}$$

$$\psi(0,t) = 0. \tag{3b}$$

In this generalized form, with the extra term $a(x)\psi$, (3a) is often referred to as the linear Ginzburg–Landau equation in the literature. At each individual location x, the system is known[31] to be locally stable if $a(x)>0$, convectively unstable if $-U_0^2/4 < a(x) < 0$ and absolutely unstable if $a(x)< -U_0^2/4$.

Cossu & Chomaz[30] considered solutions of a problem of the form (3a) that are bounded in $\mathbb{R}$, and assumed the instability parameter $a(x)$ to be of a parabolic shape $a(x) = \alpha x^2 + \beta$, with $\alpha > 0$, such that the spatial and temporal growth rates tend to $-\infty$ as $x \to \pm\infty$. Eigenmode shapes are recovered analytically, and they are found to decay as $\exp(-x^2)$ for large x.

On the contrary, if a reaches a *finite* value a_∞ as $x \to \infty$, perturbations do not experience arbitrarily strong spatial or temporal decay. For a demonstration of the spatial behavior, this limiting value a_∞ can be taken as 0 without loss of generality, as it only affects the temporal eigenvalue but not the corresponding eigenfunction. In order to model a situation where instability mechanisms are active around a given position, while passive convection and diffusion of perturbations is dominant throughout the rest of the domain, let the instability parameter $a(x)$ be of the form

$$a(x) = a_0(\mathrm{i} - 1)\mathrm{e}^{-(x-2)^2}, \quad a_0 > 0. \tag{4}$$

In order to numerically solve (3)–(4) on the interval $[0, x_{max}]$, a boundary condition has to be imposed at the outflow $x = x_{max}$. While a homogeneous Dirichlet boundary condition can be imposed for $a(x) = \alpha x^2 + \beta$ with $\alpha > 0$, this would result in the formation of a boundary layer at the outflow in our present case[32]. In order to take into account convective effects at the outflow, $\psi''(x_{max}) = 0$ is imposed. This "convective outflow"-type boundary condition neglects viscous effects at $x = x_{max}$. Results are qualitatively similar when imposing a homogeneous Neumann boundary condition, but the truncation effect is stronger.

Figure 1 shows the effect of the different parameters on the spectrum as well as on the leading eigenmode $\psi^{(0)}$. Figure 1(a) shows that, for $a_0 = 1$, the system changes from globally unstable to stable as U_0 is increased. At low values of U_0, the leading eigenmode reaches a maximum around $x = 2$ and decays exponentially downstream (figure 1(b)). As U_0 increases, the temporal decay of the mode becomes stronger, and the spatial maximum eventually disappears: exponential growth is observed essentially throughout the entire domain. As observed previously[22], the spatial growth rate of the global mode corresponds to the local spatial growth rate at the global frequency.

For $U_0 = 4$ and $U_0 = 5$, the largest values of U_0 considered in figure 1(a, b), the overall shape of the spectrum completely changes. Figure 1(b) shows that in these cases, exponential growth occurs throughout the domain, and the amplitude of the mode varies by a factor of 10^{16} between $x = 0$ and the outlet at $x = 25$: the modes, and in particular the region $1 < x < 3$ where instability mechanisms act, cannot be resolved numerically. This phenomenon can also be seen as the length of the domain is increased for fixed U_0 and a_0. The same behavior is observed for $a(x) \in \mathbb{R}$, in which case the spectrum should lie on the imaginary axis, indicating that none of these computed modes actually correspond to modes of the continuous problem. Figure 1(c) shows that the eigenvalues returned by the eigensolver for $U_0 = 5$ approximately lie on the 10^{-14} contour of the pseudospectrum of the discrete operator which, in this case, does not provide a good approximation to the spectrum. In situations where the amplitude of the mode cannot be represented throughout the domain, even the QZ algorithm fails to compute an accurate approximation to the discrete spectrum.

The relative effect of the instability parameter and of the advection velocity is summarized in figure 1(d), where the spatial growth rate of the leading eigenmode is represented as a function of the two parameters U_0 and a_0. From this growth rate, it is possible to evaluate the maximum domain length for which the computation is possible using double precision arithmetic. The dashed lines displayed in figure 1(d) correspond to values of (a_0, U_0) for which the numerical truncation errors prevented the computation.

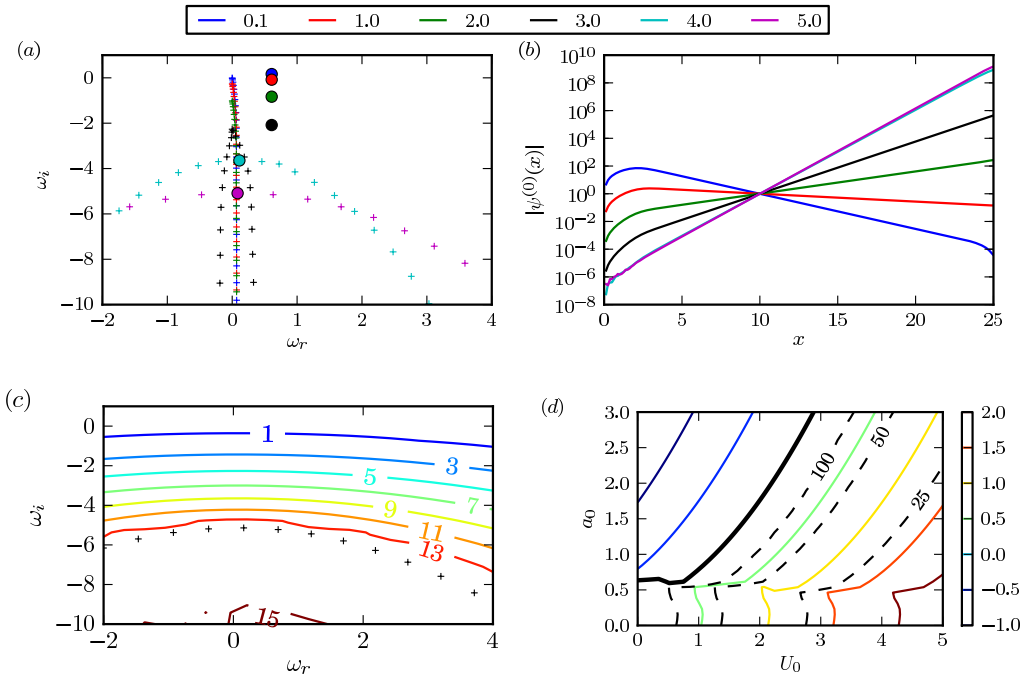

FIG. 1. (color online) (a, b): effect of U_0 on the leading eigenmodes for the advection–diffusion–reaction model (for $x_{max} = 25$ and $a_0 = 1$). The least stable part of the eigenvalue spectrum is shown in (a), and the leading eigenmode for each value of U_0 (represented in (a) by circles) are displayed in (b). (c): spectrum (+ symbols) and iso-contours of the pseudo-spectrum for $x_{max} = 25$, $U_0 = 5$ and $a_0 = 1$ (logarithmic scale). (d): Spatial growth rate of the leading global mode (measured as $\psi^{(0)'}(10)/\psi^{(0)}(10)$) as a function of parameters a_0 and U_0. The solid contour represents the limit between growing and decaying modes, the dashed lines gives the maximum value of the advection parameter for which computation is possible in a domain of a given length (indicated on the curve).

C. Conclusions from model problems

The above examples have shown that the spatial behavior to be seen in § V A for the eigenmodes of the Navier–Stokes equations is not inconsistent, and that it does not correspond to a spatial instability within a local framework. In the case where the flow dynamics are dominated by convection and diffusion effects, the downstream evolution of the modes results from two opposing mechanisms: the local stability of the flow tends to decrease the amplitude of the mode in the streamwise direction, but the advection of the globally stable structures has the opposite effect. In the case of a parabolic profile for a, the local stability eventually dominates for large x and the global modes decay to 0. On the contrary for $a \to a_0$ as $x \to \infty$ the local stability is not necessarily strong enough to prevent exponential spatial growth. The second model pointed out that, when convective effects dominate as $x \to \infty$, the size of the computational domain should be small enough that the amplitude of the mode can be resolved throughout the domain, otherwise numerical accuracy becomes problematic as the 10^{-15}-pseudospectrum can extend far from the spectrum[29]. The following section will present details on how this affects the computation and the convergence of modes for the Navier–Stokes system.

III. SETUP OF THE JET PROBLEM

A. Flow configuration

a. Incompressible setting

A cylindrical jet of a Newtonian fluid with viscosity ν^*, of radius R^* and exit velocity U_0^* is considered. The two latter quantities are used to make lengths and velocities non-dimensional. The outer fluid is at rest. The Reynolds number is taken as

$$\mathrm{Re} = \frac{U_0^* R^*}{\nu^*} = 10^3.$$

Frequencies f^* will be reported in terms of the non-dimensional circular frequency ω, related to the Strouhal number St as

$$\mathrm{St} = \frac{2 f^* R^*}{U_0^*} = \frac{\omega}{\pi}.$$

The axisymmetric flow domain, described in terms of cylindrical coordinates r, θ and x, is represented in figure 2(a). The steady solution of the non-linear Navier–Stokes equations (see § III B) is assumed to be axisymmetric. This assumption is no longer made for the perturbations, but in a linear context all perturbation quantities can be decomposed into independent Fourier-modes in θ, by introducing the azimuthal wavenumber $m \in \mathbb{N}$. Consequently, only the two-dimensional (r, x) plane needs to be discretized for both non-linear and linear calculations.

The boundary of the computational domain Ω consists of Γ_i, Γ_w,Γ_t,Γ_o and Γ_a, corresponding to the inlet, a solid wall, the outer radial boundary, the outflow and the jet axis. The inflow velocity is imposed on Γ_i, a no-slip condition on Γ_w, and stress-free boundary conditions are applied on Γ_t[33]:

$$\frac{1}{\mathrm{Re}} \frac{\partial \boldsymbol{u}}{\partial \boldsymbol{n}} - p\boldsymbol{n} = 0,$$

where $\boldsymbol{n}$ is the outgoing normal at the boundary (cf. equation 10.67 in Ref. 33). Compatibility conditions on Γ_a ensure a smooth solution on the axis[34]. Unless stated otherwise, stress-free boundary conditions are imposed at the outflow Γ_o.

The length of the pipe included in the numerical domain is set to $x_p = 5$, and it has been verified that setting the domain height to $r_{max} = 10$ does not affect the results of all incompressible calculations.

b. Compressible setting

In addition to the flow parameters introduced above, the compressible setting is characterized by density and temperature scales ρ_∞^* and T_∞^*, defined as the respective values in the outer fluid at rest. Natural choices for the Mach and Prandtl numbers are

$$\mathrm{Ma} = \frac{U_0^*}{c_\infty^*}, \qquad \mathrm{Pr} = \frac{\mu^* C_P^*}{\kappa^*},$$

where $c_\infty^* = \sqrt{\gamma r^* T_\infty^*}$ denotes the ambient speed of sound and C_p the specific heat at constant pressure.

In order to capture the acoustic radiation, the typical extent of the numerical domain has to be of the same order in the axial and radial direction. High resolution Finite Differences (FD) on a rectilinear grid are used to treat such a large problem. Consequently, the geometry (schematically displayed in figure 2(b)) is slightly different than in the incompressible case. In compressible studies, the jet pipe is modeled as an infinitely thin adiabatic wall located

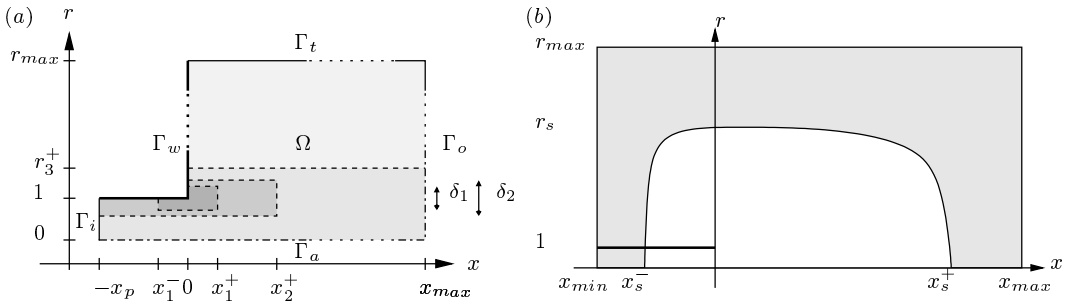

FIG. 2. Flow configuration for (a) incompressible and (b) compressible computations . The incompressible Navier–Stokes equations are solved on the 2D domain Ω using a Finite Element formulation, with an inflow boundary condition (BC) on Γ_i (thin solid line), a no slip BC on Γ_w (thick solid line), a stress-free BC on Γ_o (dashed line) and compatibility conditions on the axis Γ_a (dash-dot line). No sponge layers are used in this case. The compressible Navier–Stokes equations are discretized using high order Finite Differences (FD) on the rectangular domain represented in (b). The shaded regions correspond to sponge layers, and the presence of an infinitely thin adiabatic wall for $r = 1$ and $x \leq 0$ is taken into account by means of appropriate FD schemes.

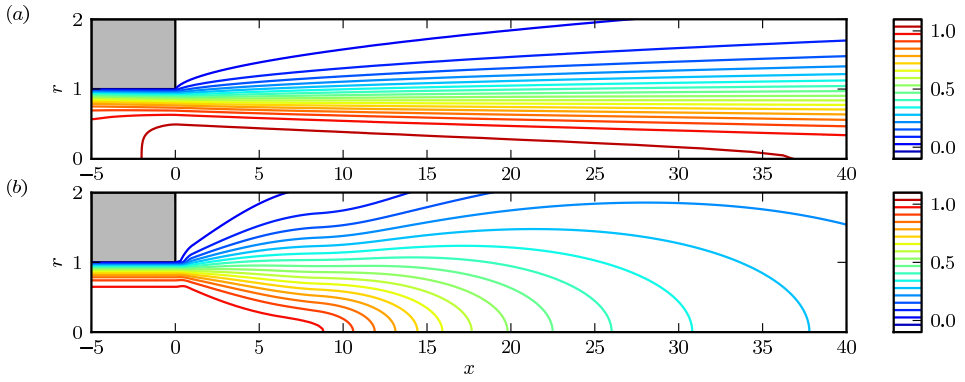

FIG. 3. Axial velocity field of the two base flows. (a) : laminar base flow, computed as a steady solution of the Navier–Stokes equations. (b) : turbulent mean flow, adapted from an analytical model[36].

at $r = 1$ and $x \leq 0$. Its presence is taken care of by using appropriate FD schemes. The treatment of the far field boundary conditions depends on the type of study performed. As will be shown later, the eigenmodes of the linearized Navier–Stokes equations are not spatially localized, so an accurate treatment of the outer boundaries is needed. To limit as much as possible the reflection of vortical or acoustic waves, the non-reflecting boundary conditions described by Bogey and Bailly[35] are used together with sponge layers. This is not required for the computation of the optimal perturbations which have a limited spatial extent. In the latter case, the sponge layers alone suffice to ensure that the solution decays to zero at the outer boundaries without affecting the flow in the physical region.

B. Base flows

Two types of base flows are investigated in this study: a laminar steady-state solution of the Navier–Stokes equations, and a parametric model of a turbulent mean flow. The incompressible analysis is performed on both these base flows, whereas only the turbulent case is considered in the compressible study.

a. Laminar steady state

A steady flow state is computed as an exact solution of the Navier–Stokes equations (see §III C). The inflow velocity is prescribed on Γ_i as

$$u_x(-x_p, r) = \tanh\left(5(1-r)\right) \qquad u_r(-x_p, r) = 0 \qquad u_\theta(-x_p, r) = 0.$$

This profile has a momentum thickness

$$\delta = \int_0^1 r u_x(1-u_x)\,\mathrm{d}r \approx \frac{1}{20}.$$

Stress-free boundary conditions are employed at the outflow Γ_o. The resulting base flow is weakly non-parallel, as seen in figure 3(a). A slight growth of the boundary layer in the pipe leads to an increase in the centerline velocity between $x = -x_p$ and 0, so that the exit centerline velocity is 1.06 at $x = 0$.

b. Turbulent mean flow

Based on experimental measurements, Monkewitz & Sohn[36] proposed a model for the turbulent mean flow of compressible jets. The flow field comprises two regions: a potential core extending over a distance of eight jet radii downstream of the nozzle, and an adjoining self-similar region with Gaussian profile shapes. This model is extended in our study by a parallel flow region inside the pipe, which smoothly connects to the free jet over the interval $0 \le x \le 1$. The full model is described in detail in Garnaud *et al.*[37]. The resulting streamwise velocity field is displayed in figure 3(b) for the zero-Mach-number case. The formulation does take into account compressibility effects, and finite-Mach-number configurations are used for the compressible analysis. The inflow momentum thickness is prescribed as $\delta^{-1} \approx 23$, similar to the laminar case.

Following Hussein & Reynolds[38], the stability of turbulent flows can be analyzed using a triple decomposition of the flow field into a mean flow, coherent perturbations and fine-scale turbulence. Using this decomposition, turbulent scales affect the motion of instability waves through Reynolds stresses, for which a closure model needs to be provided[39,40]. For turbulent jet flows, successful stability analyses[41,42] have been performed while neglecting the effect of Reynolds stresses, and this approach is also followed here as a first approximation. Local stability analyses show that perturbations with low azimuthal wavenumber m are amplified in the potential core region, whereas the self-similar downstream region of the base flow is unstable only to helical $m = 1$ perturbations.

C. Numerical methods

a. Incompressible setting

The incompressible Navier–Stokes equations are discretized using P2-P1 Finite Elements (FE), and the zero-divergence condition for the flow velocity is enforced by a penalty method[43]. The incompressible laminar steady flow is computed using Newton's method and the FreeFEM++ software[43]. A direct solver[44] is used for linear systems. Given this steady state or a model turbulent mean flow (see § III B b), the linearized Navier–Stokes equations that govern the evolution of perturbations may be written as

$$B\frac{\partial \boldsymbol{q}}{\partial t} = L\boldsymbol{q} \tag{5}$$

where $\boldsymbol{q}$ is the state vector, containing the values of all degrees of freedom of the velocity and pressure fields. Equation (5) is discretized using FreeFEM++ and the resulting sparse

matrices are exported for the linear analysis. The solution of all the problems in § IV and § V A relies on the software libraries PETSc[45], SLEPc[46] and MUMPS[44]. Eigenvalue problems arising in § V A are non-Hermitian, so the Krylov-Schur method is used. In order to compute the least stable eigenmodes the "shift-invert"[47] spectral transformation is applied using a direct linear solver.

In the study of optimal perturbations the amplitude of a perturbation needs to be measured. The square root of the perturbation kinetic energy integrated over the entire domain Ω is used for incompressible flows. This results in a pseudo-norm, as pressure is not taken into account. For the problem to be well posed, the amplitude of the initial condition needs to be measured in terms of a norm. The initial disturbance is therefore assumed to consist only of a velocity perturbation. Let $\boldsymbol{q}_u$ be a vector containing only velocity-related degrees of freedom, and P be a matrix that associates $\boldsymbol{q}_u$ to a state vector where pressure-related degrees of freedom are zero. Conversely, the operator $P^\dagger$ removes these degrees of freedom from a full state vector $\boldsymbol{q}$. The pseudo-norm is then obtained as

$$\|\boldsymbol{q}\|^2 = \boldsymbol{q}_u^\dagger Q_u \boldsymbol{q}_u = \boldsymbol{q}^\dagger P Q_u P^\dagger \boldsymbol{q} = \boldsymbol{q}^\dagger Q \boldsymbol{q} \tag{6}$$

where Q_u is a Hermitian definite matrix.

The computation of optimal perturbations described in § IV requires (i) a direct time stepper, (ii) an adjoint time stepper and (iii) an eigenvalue solver. The linear equations of motion are marched forward in time using the Crank-Nicolson method (steps (i) and (ii)). A discrete adjoint is used for step (ii), based on the Hermitian transpose of the discretization matrices. Finally, as the eigenvalue problem to be solved is Hermitian, the Lanczos method is used.

b. Compressible setting

The linearized compressible Navier–Stokes equations are spatially discretized using a finite-difference scheme designed for aero-acoustic studies[48]. The resulting discretization matrix is sparse, but with an important number of nonzero elements, in particular due to the stencil of the cross derivative terms which involves here 121 discretization points. Another consequence of the large FD stencils is that the bandwidth of the sparse discretization matrices becomes relevant, leading to excessive memory requirements for direct solvers. Iterative solvers could be used instead[49], but these methods are very sensitive to the design of an efficient preconditioner and robustness may be an issue. In order to circumvent these problems, all of the analysis is performed using an algorithm based on time stepping of linear equations (an explicit third order Runge-Kutta method is used here). In such a framework, the structure of the discretization matrices is not needed, therefore a matrix-free approach is used. Compressible eigenmodes are computed by use of a relaxation method[50], which is based on the application of a bandpass frequency filter to the equations of motion. This method allows to solve very large eigenvalue problems with low memory requirements. However, our experience shows that the relaxation method in general does not reach the machine-precision accuracy that is possible with the shift-invert method.

The adjoint Navier–Stokes operator is needed for the computation of optimal perturbations (§ IV). A discrete adjoint formulation is chosen, following the memory-efficient approach of Fosas *et al.*[51]. The norm used is that of Hanifi *et al.*[52]. Care is taken with the selective spatial filter so that the discrete propagator of the adjoint equations is the adjoint of the discrete direct propagator up to machine precision.

IV. TRANSIENT GROWTH OF PERTURBATIONS

The initial condition $\boldsymbol{q}(0)$ that is most amplified over a finite time interval T is referred to as the *optimal perturbation* for T. Reddy & Henningson[32] established the notion of optimal perturbations in order to characterize the transient (short-term) linear dynamics of flow

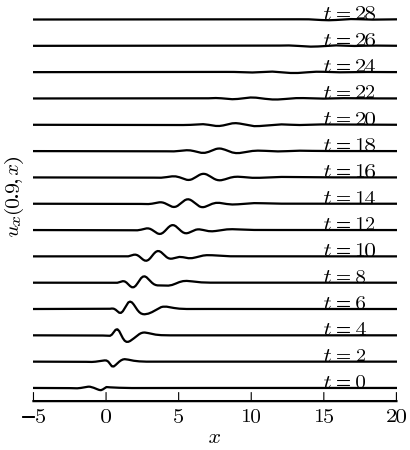

FIG. 4. Spatio-temporal evolution of the optimal initial condition for $m = 0$ and $T = 10$ for the turbulent jet mean profile in the incompressible case. The value of the axial velocity along the line $r = 0.9$ is represented at various time steps, as indicated next to the curve.

systems. Let the amplification factor be defined as

$$G_m(T) = \max_{\boldsymbol{q}(0)} \frac{\|\boldsymbol{q}(T)\|}{\|\boldsymbol{q}(0)\|} \,. \tag{7}$$

Furthermore, let $\mathcal{P}_T$ be the propagator, i.e. the linear operator that advances an initial condition over the time interval T according to equation (5). The optimal gain $G_m(T)$ is found as the leading eigenvalue of the operator $Q_u^{-1} P \mathcal{P}_T^\dagger Q \mathcal{P}_T P^\dagger$, and the associated eigenvector represents the optimal perturbation. The eigenvalue problem is solved using the Lanczos method, as implemented in the SLEPc library. The operators $\mathcal{P}_T$ and $\mathcal{P}_T^\dagger$ are applied using the time steppers described in § III C, and Q_u^{-1} is determined using a Cholesky decomposition (in the case of a finite-difference discretization, this decomposition is easily performed by hand).

A. Incompressible flow

In the incompressible setting, the length of the computational domain is chosen as $x_{max} = 40$, and stress-free boundary conditions are employed at the outflow. The convergence of the results with respect to the spatial and temporal discretizations has been verified by using (i) a halved time-step and (ii) a finer mesh where the cell size in the near-nozzle region is divided by more than 3. For both the laminar and the turbulent base flows, and for all azimuthal wave numbers and time horizons, the optimal perturbation is found in the form of structures localized in the boundary layer upstream of the nozzle, and the perturbations are amplified as they travel downstream. A typical example is shown in figure 4, which displays the evolution of the optimal perturbation of the turbulent jet for $m = 0$ and $T = 10$, along the line $r = 0.9$.

The optimal gain as a function of time horizon T is displayed in figure 5 for both base flows. In the case of the laminar base flow, this amplification factor grows monotonically with T as long as the perturbation is contained inside the numerical domain. Very large amplitudes are reached, comparable to similar computations in the supersonic regime by Nichols & Lele[17]. In the case of the turbulent base flow (figure 5(*b*)), the gain reaches a maximum for a finite time horizon $T_{opt,m}$. This maximum is particularly pronounced for axisymmetric perturbations ($m = 0$), with $T_{opt,0} \approx 10$. This interval roughly corresponds

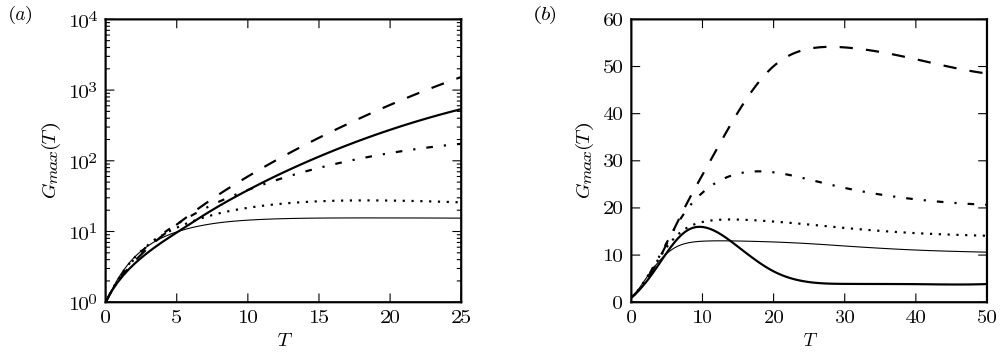

FIG. 5. Gains associated with the optimal perturbations for (a) the laminar and (b) the model base flows.Thick solid line : $m = 0$, dashed line : $m = 1$, dash-dotted line : $m = 2$, dotted line : $m = 3$ and thin solid line $m = 4$.

to the advection time of the initial perturbation across the potential core. Downstream of the potential core, axisymmetric perturbations decay as they travel on. Non-axisymmetric perturbations may still experience further growth beyond the potential core, and the decay of $G_m(T)$ with T is slower as a consequence. This observation is consistent with the fact that ~~bell-shaped~~ profiles in the self-similar regime may be unstable for $m \neq 0$ but not for axisymmetric perturbations[53]. Both the laminar and the turbulent settings display the largest gains for helical perturbations $m = 1$. It may be conjectured that a *lift-up* mechanism[54] is responsible for the strong growth of helical perturbations, since such a mechanism can only exist at azimuthal wavenumbers $m \neq 0$. However, no firm evidence of lift-up effects can be reported at present.

B. Effects of compressibility

Corresponding results of optimal perturbations of the turbulent mean flow at $Ma = 0.75$ are displayed in figure 6. The qualitative behavior of $G_{max}(T)$ (shown in figure 6(a)) is similar to that obtained for incompressible flows (figure 5(b)), and the amplification levels are comparable, although perturbations are not measured in the same norm. The spatial shape of optimal perturbations for short time horizons also resembles those found in the incompressible setting. Figures 6(b, c) show the optimal perturbation for $T = 12$: vortical structures in the pipe boundary layer are amplified as they travel through the jet shear layer. However, compressibility allows a different scenario at longer time horizons $T \gtrsim 25$, as shown in figures 6(d, e): the optimal initial condition takes the form of a spherical acoustic pulse that *contracts* and hits the nozzle at a finite time. A vortical wavepacket is thus created at the nozzle, which is amplified while it propagates through the potential core. This result illustrates that acoustic waves can be very efficiently converted into vortical perturbations at the nozzle tip[55–57].

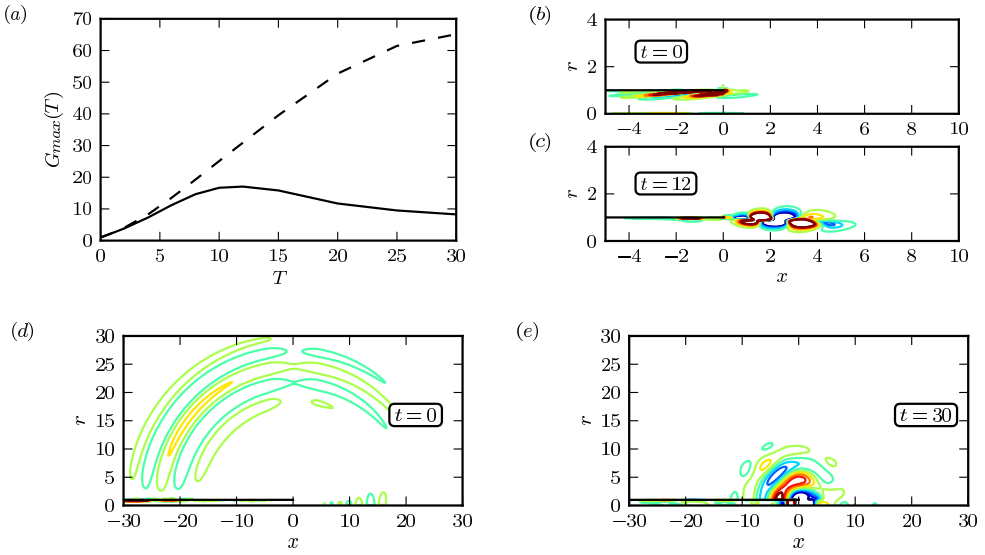

FIG. 6. (a) Optimal perturbations for the model subsonic jet at Ma $= 0.75$ for $m = 0$ (solid line) and $m = 1$ (dashed line). (b, c) : Azimuthal vorticity field for the optimal initial condition for $m = 0$ and $T = 12$, and the corresponding perturbation at $t = 12$. (d, e) : Dilatation field for the optimal initial condition for $m = 0$ and $T = 30$, and the corresponding perturbation at $t = 30$.

V. MODAL ANALYSIS

A. Incompressible global modes

a. Spectrum of the laminar base state

Eigenmodes of the linear equations (5) are sought in the form $\boldsymbol{q}(t) = \widetilde{\boldsymbol{q}}\exp(-\mathrm{i}\omega t)$, such that $\widetilde{\boldsymbol{q}}$ and ω satisfy the generalized eigenvalue problem

$$-\mathrm{i}\omega B\widetilde{\boldsymbol{q}} = L\widetilde{\boldsymbol{q}}. \tag{8}$$

Stress-free boundary conditions are used at the outflow Γ_o, and eigenmodes are computed for $x_{max} = 60$ with various shift parameters. The resulting spectra for the laminar base flow are shown in figure 7(a).

All eigenvalues have a negative growth rate $\omega_i \leq 0$ and therefore are stable. This finding is consistent with local instability results from the literature, which have shown isothermal jets to be convectively unstable[36], except in rare circumstances[58].

Several families of modes can be identified from figure 7(a). A first branch of modes, starting at the origin, is represented as circles (blue online). The least stable of these modes correspond to vortical structures in the free-stream, as displayed in figure 7(b). The wavelength of these nearly stationary modes scales with the size of the numerical domain. As the growth rate decreases along this branch, the branch is distorted and the mode structure tends to be localized more towards the jet shear-layer. This is an effect of the finite extent of the numerical domain that has been observed in other studies[26,59]. A second branch is represented by $\times$ symbols (black online). These eigenmodes are localized inside the shear layer. At the lowest frequencies, an exponential spatial growth in the streamwise direction is observed throughout the computational domain, as shown in figure 7(c). This behavior is similar to what was observed in the model problems of § II, and by this analogy we attribute the exponential spatial growth to the temporal decay of these modes. At higher frequencies (figure 7(d)), spatial growth is still found downstream of the nozzle, but the mode reaches a maximum amplitude within the computational domain. The maximum growth rate along

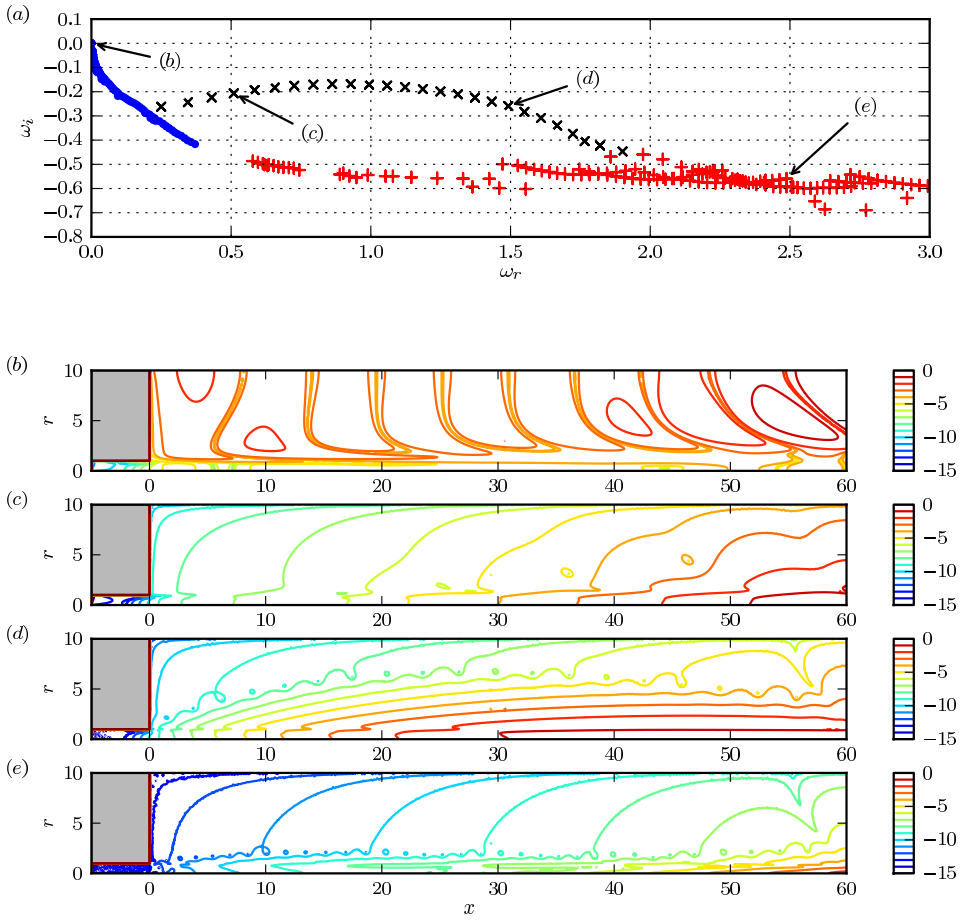

FIG. 7. Global modes computed for $m = 0$ on the laminar base flow. (a): eigenfrequency spectrum. (b, c, d, e): axial velocity magnitude of four selected modes, in logarithmic scale, as indicated in (a).

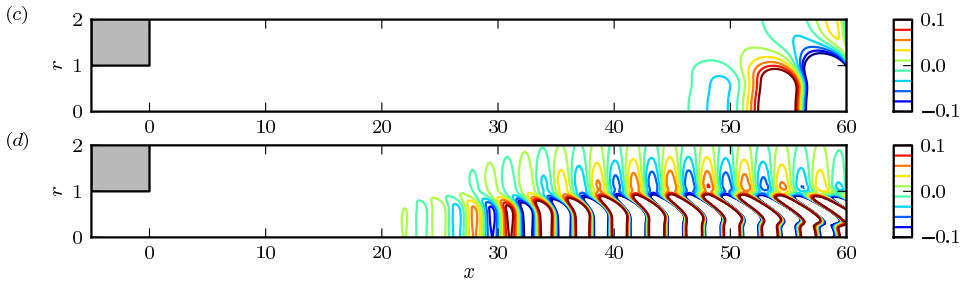

FIG. 8. Axial velocity for global modes (c) and (d) of figure 7, in linear scale.

this branch occurs around the frequency ($\omega_r \approx 1$) for which the location of maximum amplitude of the mode enters the computational domain, suggesting that the maximum in ω_i is an artifact of the finite domain size. Domain truncation effects are investigated in the following section. The phase velocity of all modes along this branch corresponds approximately to half the jet velocity on the centerline; modes at higher frequency therefore display shorter wavelengths, as can be seen in figure 8.

A third family of modes is found, represented by plus signs (red online) in figure 7(a).

None of these eigenvalues are recovered identically with different shift parameters, indicating a lack of convergence. However, these modes have been computed by the eigenvalue solver with the specified convergence criterion, namely $\|L\boldsymbol{q} + \mathrm{i}\omega\boldsymbol{q}\| < 10^{-10}\|\boldsymbol{q}\|$. We attribute this class of modes to spurious effects arising from finite machine precision. The spatial structure of one such spurious mode is represented in figure 7(e).

All modes represented in figure 7 display very large amplitude variations throughout the free-jet region. If these variations are of the order of machine precision, the low-amplitude dynamics near the nozzle cannot be accurately resolved. The perturbation amplitudes shown in figures 7($b-d$) do not span more than ten orders of magnitude in the free-jet region, and appear to be well-converged. The spurious mode in figure 7(e), in contrast, varies over 14 orders of magnitude, and seems to be affected by the double-precision round-off error as a consequence. In fact, it may be surmised that its very existence is due to the round-off error; this conjecture will be further investigated in the next section. A similar observation has been made by Heaton *et al.*[23] in their modal stability analysis of the Batchelor vortex. Those authors report that modes with amplitude variations above a factor of 10^6, between the inlet and outlet of the computational domain, cannot be accurately resolved with their numerical method. With the present algorithm, this limiting factor is approximately 10^{14}.

b. Influence of domain truncation

All eigenmodes displayed in figure 7 reach their maximum amplitude at or near the downstream boundary of the numerical domain. It may therefore be expected that the position of this boundary, as well as the numerical treatment of the outflow condition, should affect the results. In order to evaluate this influence, different domain lengths between 40 and 100 radii have been tested. The results are compared in figure 9(a), which shows that the branches of eigenmodes computed are not domain-independent. A similar behavior has been obtained in the analysis of the Blasius boundary layer[22], and is attributed to the fact that the wavepackets travel throughout the domain. Most importantly, the maximum growth rate of the shear-layer branch shifts to lower frequencies as x_{max} is increased. An inspection of the associated spatial amplitude distributions reveals that this maximum growth rate occurs roughly at the frequency at which the mode maximum amplitude is first captured inside the numerical domain. At low real frequencies, the true amplitude maximum lies on the outflow boundary of the numerical domain, and the eigenvalues are strongly affected by truncation. With increasing real frequency, this amplitude maximum moves further upstream, and the influence of the domain truncation lessens. The mode shapes shown in figure 7 are consistent with this observation. If the trend with increasing domain size is extrapolated, one may expect that the growth rate of the shear-layer branch decreases monotonically with increasing frequency in an infinitely long domain.

While the spectra in figure 9(a) have been computed with stress-free outflow conditions, figure 9(b) displays corresponding results obtained with a "convective outflow" formulation[60]. Both boundary conditions are found to give very similar results. It is inferred from this comparison that the outflow boundary conditions do not have a significant impact on the eigenmode computations in this study.

It appears that the spurious branches become less and less stable as the domain length increases. This branch is interpreted as a consequence of finite precision arithmetic. Under the assumption of a quasi-parallel flow, let C_g be the group velocity of a spurious spatial instability wave forced by numerical noise in the vicinity of the jet pipe,

$$\psi_{sp} = \widehat{\psi}(r)\exp(\mathrm{i}(k_r + \mathrm{i}k_i)x)\exp(-\mathrm{i}\omega t) \tag{9}$$

where ω is the complex forcing frequency. This forced wave will be considered an eigenmode by the solver if the forcing amplitude is of the order of the numerical precision ϵ_m, i.e. if the amplitudes of this forced wave at the inlet and at the outlet are such that

$$\psi(x=0) \sim \epsilon_m \psi(x = x_{max}).$$

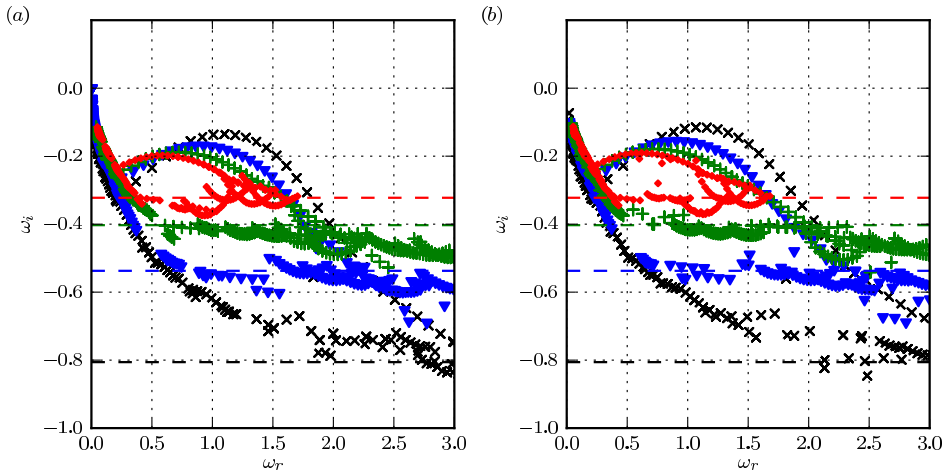

FIG. 9. Spectra computed for various domain lengths using stress-free (a) and convective outflow (b) boundary conditions at the outlet. Crosses : $x_{max} = 40$ (black online). Triangles : $x_{max} = 60$ (blue online). Plusses : $x_{max} = 80$ (green online). Circles : $x_{max} = 100$ (red online). The dashed lines corresponds to the estimated decay rate (11).

In this case, (9) gives $k_i = -\log(\epsilon_m)/x_{max}$. Let $\omega_i^t(k_r)$ be the local temporal growth rate associated with the axial wavenumber k_r. In the limit of long wavelengths, jet flow profiles are approximately marginally stable. Following an approach similar to that of the Gaster transformation[61], the global temporal decay rate ω_i can be related to the global spatial growth rate k_i by

$$\omega_i \approx C_g k_i + \omega_i^t(k_r) \approx C_g \frac{\log(\epsilon_m)}{x_{max}}. \tag{10}$$

As the group velocity C_g is of the order of the base flow velocity U_0, the decay rate associated with such pseudomodes can be estimated as

$$\sigma \equiv U_0 \frac{\log(\epsilon_m)}{x_{max}}. \tag{11}$$

Figure 9 shows that the above expression provides a reasonable estimate for the decay rate of the spurious modes. Since σ varies as $1/x_{max}$, this spurious branch will eventually become less stable than the other two branches as x_{max} increases, preventing their computation. It is thus impossible to obtain converged results for the spectra, at least using standard double precision arithmetic ($\epsilon_m = 10^{-15}$).

It appears that machine precision imposes severe constraints on global mode computations for convective flows such as jets. The streamwise extent of the numerical domain must be sufficiently large to capture the amplitude maximum of the mode, but the amplitude variations must also be within the range of machine precision. At the same time, spurious modes contaminate an increasingly large portion of the spectrum as the numerical domain length is increased.

c. Spectrum of the turbulent mean flow

One may intuitively expect that the much faster spreading of the turbulent mean flow, compared to the laminar base flow considered in the last section, will lead to global mode structures that decay spatially within a shorter distance from the nozzle. In view of the

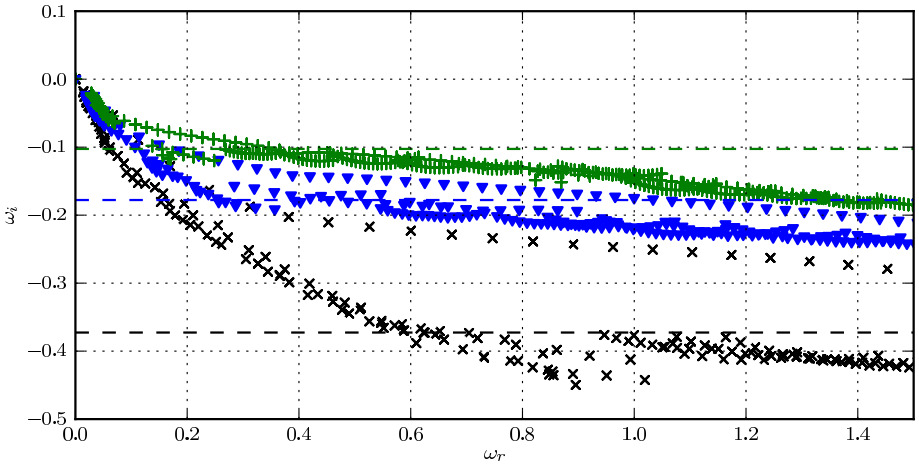

FIG. 10. Global spectra computed for $m = 0$ for the model base flow. Crosses : $x_{max} = 40$ (black online). Triangles : $x_{max} = 60$ (blue online). Plusses : $x_{max} = 80$ (green online). The dashed lines corresponds to the estimated decay rate of the spurious branch given by (11).

discussion in the preceeding section, such a behavior would be favorable for the numerical analysis. However, the mean flow spreading also implies a decreased advection velocity, which in turn strengthens the spatial growth due to the advection of stable structures.The estimate for the decay rate of spurious structures given by (11) can be modified to account for the significant variation of the base velocity on the jet axis, giving

$$\sigma' \equiv \log(\epsilon_m) \left(\int_0^{x_{max}} \frac{1}{u_x^0(0,x)} \, \mathrm{d}x \right)^{-1} . \tag{12}$$

The spectra displayed in figure 10 show that this estimate is also reasonably accurate. This implies an even more stringent constraint on the size of the computational domain than in the case of a nearly parallel flow.

Figure 11 displays selected global modes computed for $x_{max} = 60$: as for all the modes presented in figure 10, the exponential growth continues throughout the computational domain. Indeed, in light of the discussion of the model problems, there is no guarantee that a maximum will ever be reached: the maximum amplitude may well continue towards infinity. Against all expectations, it is found that the faster spreading of the present mean flow does not lead to more upstream-localized mode structures. Therefore the computation of the spectrum is *not* any more accessible than in the laminar base flow case.

B. Compressible eigenmodes

Eigenmodes have been computed for the model mean flow at Ma = 0.75. The computed spectrum is displayed in figure 12(a). Similar to the incompressible case, it is worth pointing out that the spectrum does not show any preferred frequency. The decay rates of the modes are however significantly less stable than in the incompressible case, by more than a factor of five. Although the solver used for this computation is less accurate than the one used for incompressible computations, the results displayed in figure 12 are converged with respect to the iterative eigenvalue solver. As a consequence of the very low decay rate, the spatial growth of eigenmodes is weaker than in the incompressible case, and at high frequencies the global modes decay right after the end of the jet pipe (see figure 12(b, c, d))

Several reasons may explain such a slow temporal decay. As it was seen in § IV, acoustic disturbances efficiently excite vortical structures, and, as the Mach number increases, the

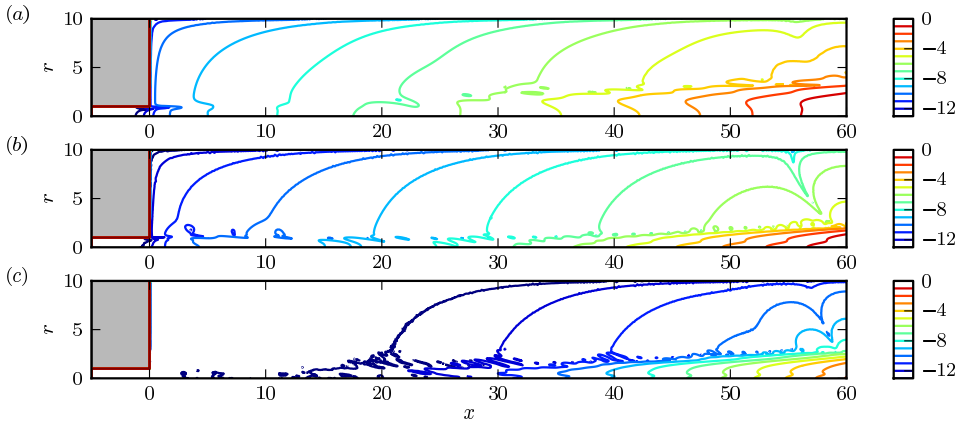

FIG. 11. Axial velocity fields of selected global modes computed for $m = 0$ for the model base flow with $x_{max} = 60$ and stress-free outflow boundary conditions (logarithmic scale). (a) : $\omega = 0.22 - 0.11\mathrm{i}$, (b) : $\omega = 1.0 - 0.17\mathrm{i}$, (c) : $\omega = 0.98 - 0.23\mathrm{i}$.

acoustic wavelength gets closer to the wavelength of vortical wavetrains, so that excitation can be efficient and lead to a feedback loop. The feedback could also be spurious: indeed, although the optimal perturbation results of § IV are quite insensitive to the treatment of the outer boundaries, this significantly affects the eigenmodes. In spite of the use of non-reflecting boundary conditions and very weak sponge regions, it is expected that an effect is still present here. Similarly, as the vorticity field grows in space due to the temporal stability, the acoustic field also grows exponentially with the distance to the acoustic sources. As a consequence, even for weakly damped modes, reflection can be significant in large numerical domains. Finally, the low decay rate may be related to the fact that the numerical dissipation is lower with the present FD formulation than with the FE discretization used for incompressible flows. Indeed, in situations where structures are convected outside of the numerical domain, dissipative effects can be important at large times.

VI. PROJECTION OF THE TRANSIENT DYNAMICS ONTO THE SPACE SPANNED BY EIGENMODES.

Optimal perturbations have been computed in § IV using a direct-adjoint technique. An alternative method is to approximate the propagator using a reduced-order basis consisting of the computed eigenmodes. This technique has, for example, been successfully used by Akervik *et al*[7] for the global analysis of an amplifier flow. Regardless of the relevance of the eigenmodes to describe the dynamics, such an analysis is expected to yield accurate results provided the eigenmodes are computed accurately. Figure 13 displays the optimal gains computed for the laminar incompressible jet with $m = 0$: the N least stable eigenmodes have been used for the computation, with N varying from 5 to 183[62]. It appears that even when all the computed eigenmodes are taken into account, the optimal gains are under-estimated by up to two orders of magnitude. Eigenmodes are therefore not relevant individually, which is already well known for amplifier flows, but also as a superposition to represent transient dynamics. A similar study on a stable lid-driven cavity flow (not shown here) yielded substantially better convergence towards transient energy gains when the number of included eigenmodes is increased. This further emphasized the role of advection in the representation of transient phenomena by global modes. The above finding is contrary to that of Akervik *et al*[7] and is related to the much stronger streamwise growth of eigenmodes in the present configuration. Indeed the optimal initial conditions consist of structures in the jet pipe. In this region, all eigenmodes have very small amplitudes and numerical inaccuracies

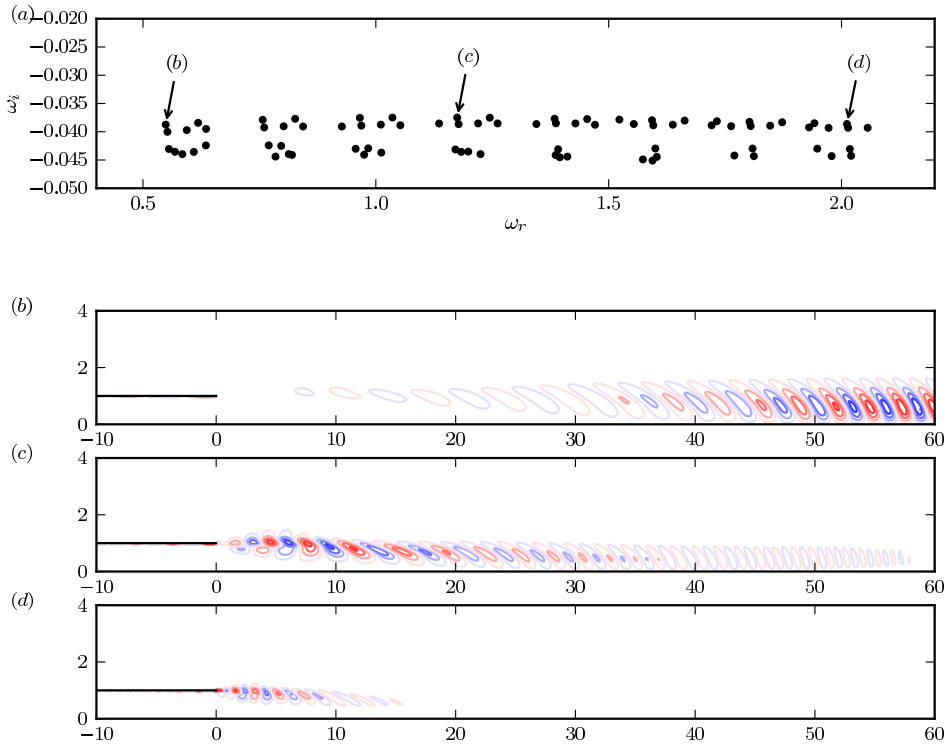

FIG. 12. Global modes computed for $m = 0$ on the model subsonic jet at Ma $= 0.75$. (a): eigenvalue spectrum. (b, c, d): azimuthal vorticity of three selected modes, as indicated in (a).

(due to both the eigenmode computation and the projection) become significant.

VII. CONCLUSIONS

The linear dynamics of perturbations in jet flows is the result of two mechanisms, advection by the base flow and shear layer instability. In order to investigate the effect of these two features on the modal and non-modal stability properties of the flow, two types of base flows have been considered. The first one is a laminar steady solution of the Navier–Stokes equation, for which both advection and instability remain approximately constant in the streamwise direction. A turbulent mean flow has also been used: in this case, instability is limited to a region of about eight radii downstream of the jet pipe, referred to as the potential core, where advection remains approximately constant. Further downstream the base flow velocity decreases significantly and the jet profiles become stable to axisymmetric perturbations.

An optimal perturbation analysis has been performed on these two base flows, revealing that vortical structures are amplified throughout the laminar jet, but only in the potential core for turbulent mean flows. In both cases the flow is globally stable.

In order to investigate the preferred frequency observed in jet experiments, a modal analysis has then been performed, but several difficulties were encountered. The eigenmodes, computed on a finite domain, exhibit an exponential growth in the streamwise direction. Intuitively, one might expect that eigenmodes should spatially decay in locally stable flow regions, and that therefore such a decay will eventually occur if the numerical domain is long enough in the streamwise direction. This is actually not the case, and longer computational domains in fact tend to aggravate the numerical difficulties.

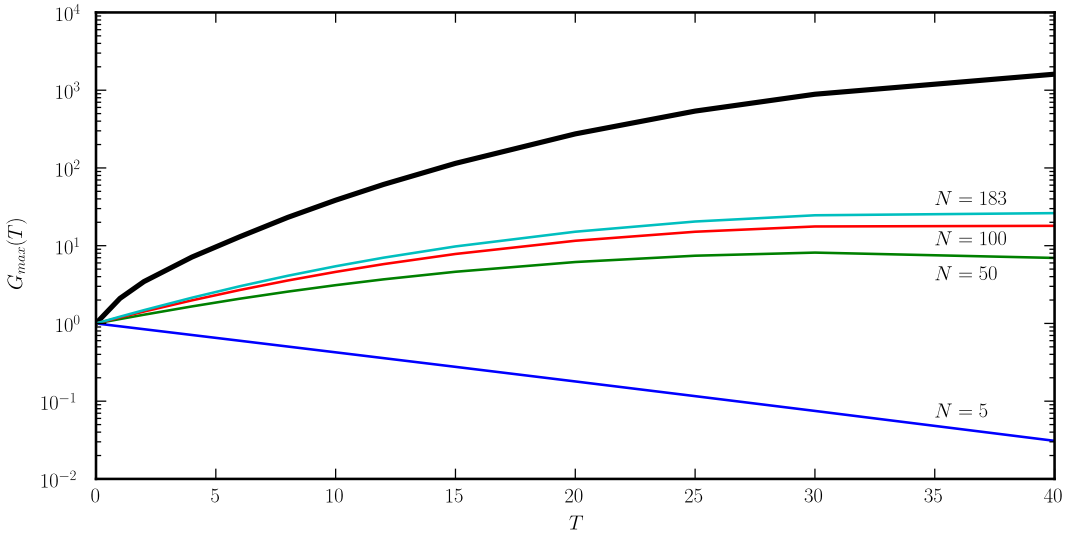

FIG. 13. Optimal transient amplification of axisymmetric perturbations for the laminar incompressible jet. Thick line: computation using the adjoint equations, as computed in § IV. Thin lines: optimal gains computed by projecting the dynamics onto the space spanned by the N least stable eigenmodes.

The cause of these problems has been discussed for model equations that mimic the advection and instability properties of jet flows. Indeed, when eigenmodes represent the advection of stable, temporally decaying structures, they grow exponentially in the streamwise direction. When computing such modes, difficulties therefore arise due to the domain truncation, the modeling of outflow boundary conditions and the finite precision of computer arithmetic.

Eigenmodes have been computed for jets in laminar and turbulent, compressible and incompressible settings, and results display the same properties as those obtained from the model problems. It has been shown that convergence of the spectrum of incompressible jets is inhibited by the presence of spurious pseudomodes which impose strict constraints on the size of the numerical domain.

As was shown with simple models, the exponential spatial growth of the stable modes is not an indication of a local spatial instability, it is merely a reflection of the fact that the eigenfrequency ω has a negative imaginary part. This has been further exemplified through the computation of eigenmodes for turbulent mean flows that grow even faster than those computed for a laminar base flow while the flow is stable downstream of the potential core for $m = 0$. The temporally stable structures observed in the modes, generated by a shear layer instability downstream of the nozzle, are convected downstream in a quasi-neutral flow resulting in an apparent spatial growth. For both mean flows the global decay rates of shear layer modes are of the same order of magnitude since the inflow shear layer thickness is similar. As the advection velocity is much smaller for the turbulent mean flow, the spatial growth is therefore larger.

For compressible flows, the computed eigenmodes are less stable than in the incompressible case. As a consequence, the local stability of shear layer structures dominates over the growth due to stable advection such that the exponential growth is not observed. However, this growth not only affects vortical structures but also acoustic waves. For acoustic perturbations the exponential growth due to the advection of stable structures eventually dominates over the algebraic decay: the acoustic waves radiated from a mode reach their maximum amplitude at the boundaries of the computational domain, which represents considerable challenges to avoid spurious reflections.

The present results found for jet flows are consistent with the literature on the stability of the Blasius boundary layer. The qualitative features of the eigenmodes are similar for jets and boundary layers, but the physical settings are quite different, and eigenmodes are much

less temporally stable for the boundary layer problem. Consequently, the spatial growth of boundary layer modes is weaker and numerical issues are less important than in the jet configuration.

All the numerical challenges faced in the modal analysis of jet flows cannot be attributed to a poor discretization and other numerical influence, since the numerical tools used in this study provided robust results for the transient flow analysis. As the numerical schemes employed for this study are linear, the transient simulations can be viewed as a superposition of all eigenmodes of the discrete problem. The issues are not related to the convective nature of the flow, since the transient analysis successfully and robustly reproduced the flow behavior; they rather lie with the description of stable convective dynamics by global modes, and their interpretation as coherent invariant structures.

ACKNOWLEDGMENTS

This work was supported by DGA grant number 2009.60.034.00.470.75.01 and by a fellowship from the EADS Foundation. Calculations were performed using HPC resources from GENCI (Grant 2012-026451). The authors thank F. Gallaire for his help.

[1]D. Barkley, "Linear analysis of the cylinder wake mean flow," Europhysics Letters **75**, 750–756 (2006) doi:10.1209/epl/i2006-10168-7.

[2]S. Bagheri, P. Schlatter, P. Schmid, and D. Henningson, "Global stability of a jet in crossflow," Journal of Fluid Mechanics **624**, 33 (2009) doi:10.1017/S0022112009006053.

[3]U. Ehrenstein and F. Gallaire, "Two-dimensional global low-frequency oscillations in a separating boundary-layer flow," Journal of Fluid Mechanics **614**, 315 (2008) doi:10.1017/S0022112008003285.

[4]P. Meliga, J. Chomaz, and D. Sipp, "Global mode interaction and pattern selection in the wake of a disk: a weakly nonlinear expansion," Journal of Fluid Mechanics **633**, 159 (2009) doi:10.1017/S0022112009007290.

[5]M. Navarro, L. Witkowski, L. Tuckerman, and P. L. Quéré, "Building a reduced model for nonlinear dynamics in Rayleigh-Bénard convection with counter-rotating disks," Physical Review E **81** (2010) doi: 10.1103/PhysRevE.81.036323.

[6]O. Marquet, D. Sipp, and L. Jacquin, "Sensitivity analysis and passive control of cylinder flow," Journal of Fluid Mechanics **615**, 221–252 (2008) doi:10.1017/S0022112008003662.

[7]E. Akervik, J. Hoepffner, U. Ehrenstein, and D. Henningson, "Optimal growth, model reduction and control in a separated boundary-layer flow using global eigenmodes," Journal of Fluid Mechanics **579**, 305 (2007) doi:10.1017/S0022112007005496 .

[8]A. Barbagallo, D. Sipp, and P. Schmid, "Inputoutput measures for model reduction and closed-loop control: application to global modes," Journal of Fluid Mechanics **685**, 23–53 (2011) doi:10.1017/jfm.2011.271.

[9]P. Huerre and P. Monkewitz, "Local and global instabilities in spatially developing flows," Annual Review of Fluid Mechanics **22**, 473–537 (1990) doi:10.1146/annurev.fl.22.010190.002353.

[10]J. Chomaz, "Global instabilities in spatially developing flows: Non-Normality and nonlinearity," Annual Review of Fluid Mechanics **37**, 357–392 (2005) doi:10.1146/annurev.fluid.37.061903.175810.

[11]L. Lesshafft, P. Huerre, P. Sagaut, and M. Terracol, "Nonlinear global modes in hot jets," Journal of Fluid Mechanics **554**, 393–409 (2006) doi:10.1017/S0022112006008974.

[12]L. Lesshafft, P. Huerre, and P. Sagaut, "Frequency selection in globally unstable round jets," Physics of Fluids **19**, 054108 (2007) doi:10.1063/1.2732247.

[13]S. Crow and F. Champagne, "Orderly structure in jet turbulence," Journal of Fluid Mechanics **48**, 547 (1971) doi:10.1017/S0022112071001745 .

[14]D. Bodony and S. Lele, "On using large-eddy simulation for the prediction of noise from cold and heated turbulent jets," Physics of Fluids **17**, 085103 (2005) doi:10.1063/1.2001689.

[15]A. Cooper and D. Crighton, "Global modes and superdirective acoustic radiation in low-speed axisymmetric jets," European Journal of Mechanics - B/Fluids **19**, 559–574 (2000) doi:10.1016/S0997-7546(00)90101-8.

[16]C. Moore, "The role of shear-layer instability waves in jet exhaust noise," Journal of Fluid Mechanics **80**, 321 (1977) doi:10.1017/S0022112077001700.

[17]J. Nichols and S. Lele, "Non-normal global modes of high-speed jets," International Journal of Spray and Combustion Dynamics **3**, 285–302 (2011) doi:10.1260/1756-8277.3.4.285.

[18]J. Nichols and S. Lele, "Global mode analysis of turbulent high-speed jets," Annual Research Briefs 2010 (Center for Turbulence Research, 2010).

[19]D. Barkley, M. Gomes, and R. Henderson, "Three-dimensional instability in flow over a backward-facing step," Journal of Fluid Mechanics **473** (2002) doi:10.1017/S002211200200232X.

[20]O. Tammisola, *Linear stability of plane wakes and liquid jets: global and local approach*, PhD thesis, KTH (2009).

[21]O. Tammisola, F. Lundell, and L. Soderberg, "Effect of surface tension on global modes of confined wake flows," Physics of Fluids **23**, 014108 (2011) doi:10.1063/1.3540686.

[22]U. Ehrenstein and F. Gallaire, "On two-dimensional temporal modes in spatially evolving open flows: the flat-plate boundary layer," Journal of Fluid Mechanics **536**, 209–218 (2005) doi: 10.1017/S0022112005005112.
[23]C. Heaton, J. Nichols, and P. Schmid, "Global linear stability of the non-parallel batchelor vortex," Journal of Fluid Mechanics **629**, 139 (2009) doi:10.1017/S0022112009006399.
[24]L. Trefethen, A. Trefethen, S. Reddy, and T. Driscoll, "Hydrodynamic stability without eigenvalues," Science **261**, 578–584 (1993) doi:10.1126/science.261.5121.578.
[25]P. Schmid, "Nonmodal stability theory," Annual Review of Fluid Mechanics **39**, 129–162 (2007) doi: 10.1146/annurev.fluid.38.050304.092139.
[26]E. Akervik, U. Ehrenstein, F. Gallaire, and D. Henningson, "Global two-dimensional stability measures of the flat plate boundary-layer flow," European Journal of Mechanics - B/Fluids **27**, 501–513 (2008) doi:10.1016/j.euromechflu.2007.09.004.
[27]B. Farrell and A. Moore, "An adjoint method for obtaining the most rapidly growing perturbation to oceanic flows," Journal of Physical Oceanography **22**, 338–349 (1992) doi:10.1175/1520-0485(1992)022¡0338:AAMFOT¿2.0.CO.
[28]K. Butler and B. Farrell, "Three-dimensional optimal perturbations in viscous shear flow," Physics of Fluids A: Fluid Dynamics **4**, 1637 (1992) doi:10.1063/1.858386.
[29]S. Reddy and L. Trefethen, "Pseudospectra of the Convection-Diffusion operator," SIAM Journal on Applied Mathematics **54**, 1634 (1994).
[30]C. Cossu and J. Chomaz, "Global measures of local convective instabilities," Physical Review Letters **78**, 4387–4390 (1997) doi:10.1103/PhysRevLett.78.4387.
[31]P. Huerre and P. Monkewitz, "Absolute and convective instabilities in free shear layers," Journal of Fluid Mechanics **159**, 151–168 (1985) doi:10.1017/S0022112085003147.
[32]S. Reddy and D. Henningson, "Energy growth in viscous channel flows," Journal of Fluid Mechanics **252**, 209–238 (1993) doi:10.1017/S0022112093003738.
[33]E. Dick, "Introduction to finite element methods in computational fluid dynamics," in *Computational Fluid Dynamics*, edited by J. Wendt (Springer Berlin Heidelberg, 2009) pp. 235–274 doi:10.1007/978-3-540-85056-4˙10.
[34]T. Matsushima and P. Marcus, "A spectral method for polar coordinates," Journal of Computational Physics **120**, 365–374 (1995) doi:10.1006/jcph.1995.1171.
[35]C. Bogey and C. Bailly, "Three-dimensional non-reflective boundary conditions for acoustic simulations: far field formulation and validation test cases," Acta Acustica **88**, 463–471 (2002).
[36]P. Monkewitz and K. Sohn, "Absolute instability in hot jets," AIAA Journal **26**, 911–916 (1988) doi: 10.2514/3.9990.
[37]X. Garnaud, L. Lesshafft, and P. Huerre, "Global linear stability of a model subsonic jet," AIAA paper 2011-3608 (2011).
[38]W. Reynolds and A. Hussain, "The mechanics of an organized wave in turbulent shear flow. part 3. theoretical models and comparisons with experiments," Journal of Fluid Mechanics **54**, 263 (1972) doi: 10.1017/S0022112072000679.
[39]V. Kitsios, L. Cordier, J. Bonnet, A. Ooi, and J. Soria, "Development of a nonlinear eddy-viscosity closure for the triple-decomposition stability analysis of a turbulent channel," Journal of Fluid Mechanics **664**, 74–107 (2010) doi:10.1017/S0022112010003617 .
[40]J. Crouch, A. Garbaruk, and D. Magidov, "Predicting the onset of flow unsteadiness based on global instability," Journal of Computational Physics **224**, 924–940 (2007) doi:10.1016/j.jcp.2006.10.035.
[41]D. Crighton and M. Gaster, "Stability of slowly diverging jet flow," Journal of Fluid Mechanics **77**, 397 (1976) doi:10.1017/S0022112076002176.
[42]K. Gudmundsson and T. Colonius, "Instability wave models for the near-field fluctuations of turbulent jets," Journal of Fluid Mechanics **689**, 97–128 (2011) doi:10.1017/jfm.2011.401.
[43]F. Hecht, "Freefem++ manual, third edition, version 3.16-1," Tech. Rep. (2011) université Pierre et Marie Curie, Paris, France.
[44]P. Amestoy, I. Duff, and J. L'Excellent, "Multifrontal parallel distributed symmetric and unsymmetric solvers," Computational Methods in Applied Mathematics **184**, 501–520 (2000).
[45]S. Balay, K. Buschelman, V. Eijkhout, W. Gropp, D. Kaushik, M. Knepley, L. C. McInnes, B. Smith, and H. Zhang, "PETSc users manual," Tech. Rep. ANL-95/11 - Revision 3.0.0 (Argonne National Laboratory, 2008) mathematics and Computer Science Division, Argonne National Laboratory, USA.
[46]V. Hernandez, J. Roman, and V. Vidal, "SLEPc: a scalable and flexible toolkit for the solution of eigenvalue problems," ACM Transactions on Mathematical Software **31**, 351362 (2005).
[47]R. Lehoucq, D. Sorensen, and C. Yang, *ARPACK Users' Guide: Solution of Large-Scale Eigenvalue Problems with Implicitly Restarted Arnoldi Methods* (SIAM, 1998).
[48]C. Bogey and C. Bailly, "A family of low dispersive and low dissipative explicit schemes for flow and noise computations," Journal of Computational Physics **194**, 194–214 (2004) doi:10.1016/j.jcp.2003.09.003.
[49]C. Mack and P. Schmid, "A preconditioned krylov technique for global hydrodynamic stability analysis of large-scale compressible flows," Journal of Computational Physics **229**, 541–560 (2010) doi: 10.1016/j.jcp.2009.09.019.
[50]X. Garnaud, L. Lesshafft, P. Schmid, and J. Chomaz, "A relaxation method for large eigenvalue problems, with an application to flow stability analysis," Journal of Computational Physics (2012) doi: 10.1016/j.jcp.2012.01.038, .

[51]M. Fosas de Pando, D. Sipp, and P. Schmid, "Efficient evaluation of the direct and adjoint linearized dynamics from compressible flow solvers," Journal of Computational Physics **231**, 7739–7755 (2012) doi: 10.1016/j.jcp.2012.06.038.
[52]A. Hanifi, P. Schmid, and D. Henningson, "Transient growth in compressible boundary layer flow," Physics of Fluids **8**, 826–837 (1996) doi:10.1063/1.868864.
[53]A. Michalke, "Survey on jet instability theory," Progress in Aerospace Science **21**, 159–199 (1984) doi: 10.1016/0376-0421(84)90005-8.
[54]M. Landahl, "A note on an algebraic instability of inviscid parallel shear flows," Journal of Fluid Mechanics **98**, 243 (1980) doi:10.1017/S0022112080000122.
[55]D. Jones and J. Morgan, "The instability of a vortex sheet on a subsonic stream under acoustic radiation," Mathematical Proceedings of the Cambridge Philosophical Society **72**, 465 (1972) doi: 10.1017/S0305004100047320.
[56]D. Crighton and F. Leppington, "Radiation properties of the semi-infinite vortex sheet: the initial-value problem," Journal of Fluid Mechanics **64**, 393 (1974) doi:10.1017/S0022112074002461.
[57]M. Barone and S. Lele, "Receptivity of the compressible mixing layer," Journal of Fluid Mechanics **540**, 301–335 (2005) doi:10.1017/S0022112005005884.
[58]L. Lesshafft, P. Huerre, and P. Sagaut, "Aerodynamic sound generation by global modes in hot jets," Journal of Fluid Mechanics **647**, 473–489 (2010) doi:10.1017/S0022112009993612.
[59]P. Schmid and D. Henningson, *Stability and Transition in Shear Flows* (Springer, New York, 2001) doi: 10.1115/1.1470687.
[60]I. Orlanski, "A simple boundary condition for unbounded hyperbolic flows," Journal of Computational Physics **21**, 251–269 (1976) doi:10.1016/0021-9991(76)90023-1.
[61]W. Criminale, T. Jackson, and R. Joslin, *Theory and computation of hydrodynamic stability* (Cambridge University Press, Cambridge, UK, 2003) doi:10.1017/CBO9780511550317.
[62]For $m = 0$ the linearized Navier–Stokes operator is real, so only eigenvalues with $\omega_r \geq 0$ need to be considered.